Editors' Suggestion

Sound speed and Grüneisen parameter up to three terapascal in shock-compressed iron

M. F. Huff,[1,2] D. E. Fratanduono,[3] M. C. Marshall,[1] C. A. McCoy,[4] L. E. Hansen,[1,2] D. N. Polsin,[1,5] T. Suer,[1] E. A. Smith,[1,2] B. J. Henderson,[1,2] X. Gong,[1,5] G. W. Collins,[1,2,5] and J. R. Rygg[1,2,5]

[1]*Laboratory for Laser Energetics, University of Rochester, Rochester, New York 14623, USA*

[2]*Department of Physics and Astronomy, University of Rochester, Rochester, New York 14627, USA*

[3]*Lawrence Livermore National Laboratory, Livermore, California 94550-9234, USA*

[4]*Sandia National Laboratories, Albuquerque, New Mexico 87185, USA*

[5]*Department of Mechanical Engineering, University of Rochester, Rochester, New York 14627, USA*

(Received 17 December 2022; revised 26 May 2023; accepted 24 April 2024; published 22 May 2024)

This paper presents the first sound speed and Grüneisen parameter data for fluid iron compressed to 3 TPa (30 million atmospheres) and 20 g/cm^3 on the Hugoniot. Both the sound speed and Grüneisen parameter are derivatives of the equation of state (EOS) and thus tightly constrain the contours of the EOS surface. The sound speed data are systematically lower than expected from a simple extrapolation of previous data. The Grüneisen parameter shows a 30% drop at pressures and temperatures above the melt transition. Furthermore, while some models compare well with either the sound speed or Grüneisen parameter, none of today's state-of-the-art models can explain both sets of data. Thus these new data will provide pivotal benchmarks for both future theoretical EOSs of warm dense iron and modeling planetary states and processes.

DOI: 10.1103/PhysRevB.109.184311

I. INTRODUCTION

Iron is an abundant element, widely studied in astrophysics [1–3], in planetary physics [4–7], and for industrial purposes. Prompted by the discovery of numerous large rocky exoplanets with expected iron cores [8] and measurements of Jupiter's gravitational field suggesting iron might be spread throughout a diffuse core [9], significant effort is underway to understand the equation of state (EOS) of iron in the terapascal range [10,11].

While the pressure-density relationship for iron has been well studied both on the Hugoniot and the isentrope [12–22], modeling planetary processes (i.e., giant impacts or core formation) often relies on little studied derivative quantities such as Grüneisen parameter and sound speed to determine subtle contour changes in the EOS surface as well as the entropy and thermal pressure [2,23]. This study provides benchmark data for theoretical calculations [24–26] and simulations [27,28] for the iron EOS in the warm dense matter (WDM) regime, where typical approximations for the hot plasma phase or the lower temperature solid state are not appropriate. The warm dense matter regime is where several energy scales are comparable, including the Coulomb interaction energy E_c, thermal energy k_BT (where k_B is Boltzmann's constant and T is the temperature), and the Fermi energy E_F. For the data presented here, the electron-electron coulomb coupling ratio ($\Gamma_{ee} = \frac{E_c}{k_BT}$) spans 1.6 to 4.7, revealing the importance of coulomb interactions. The degeneracy parameter, $\Theta = \frac{k_BT}{E_F}$, spans 0.5 to 0.2, suggesting iron studied here is also moderately degenerate.

The fluid bulk sound speed $c_s = \sqrt{\frac{dP}{d\rho}|_S}$, with P = pressure, ρ = density, and S = entropy, can be related to the bulk modulus B_S as $c_s = \sqrt{\frac{B_S}{\rho}}$ and thus c_s is related to a materials resistance to compression. The Grüneisen parameter, $\gamma = V\frac{dP}{dE}|_V = -\frac{\partial \ln T}{\partial \ln V}|_S$, where E = energy and V = volume, describes how pressure changes with thermal energy [11,23,29,30].

High pressure c_s data have been collected through a variety of experimental techniques including velocimetry [31–35], pyrometry [16], and radiography [36], and are used in the interpretation of seismological events [37], in giant impact simulations [38,39], and in compositional studies of Earths core [4,40,41]. Grüneisen parameter can be determined from both seismological studies [42,43] and laboratory experiments such as x-ray diffraction [30], measurements of heat capacity and elastic constants [4], Hugoniot measurements on different density samples [44,45], and sound speed measurements from dynamic compression experiments [11,16,31]. Previous iron c_s and γ data are limited to ~800 GPa on the Hugoniot [17,36] and 1.2 TPa on a quasi-isentropic path [11]. The work presented here extends the database for these derivative quantities in the fluid regime by nearly 4 times in pressure.

The iron shock Hugoniot, together with the sound speed and Grüneisen parameter data, are presented to 3 TPa, where the current state of the art models [24–26] are disparate. Based on estimates from these models, the pressure range of 500–3700 GPa corresponds to a temperature range of 6000–80 000 K. Of particular interest is the Grüneisen parameter, which has a significant dependence on temperature, especially in the vicinity of the melting transition, and the sound speed in the TPa regime is significantly lower than expected from previous lower pressure measurements [36].

II. EXPERIMENTAL TECHNIQUE

This work utilizes a method to create a nearly-steady shock wave with imposed acoustic perturbations [Fig. 1(b)]

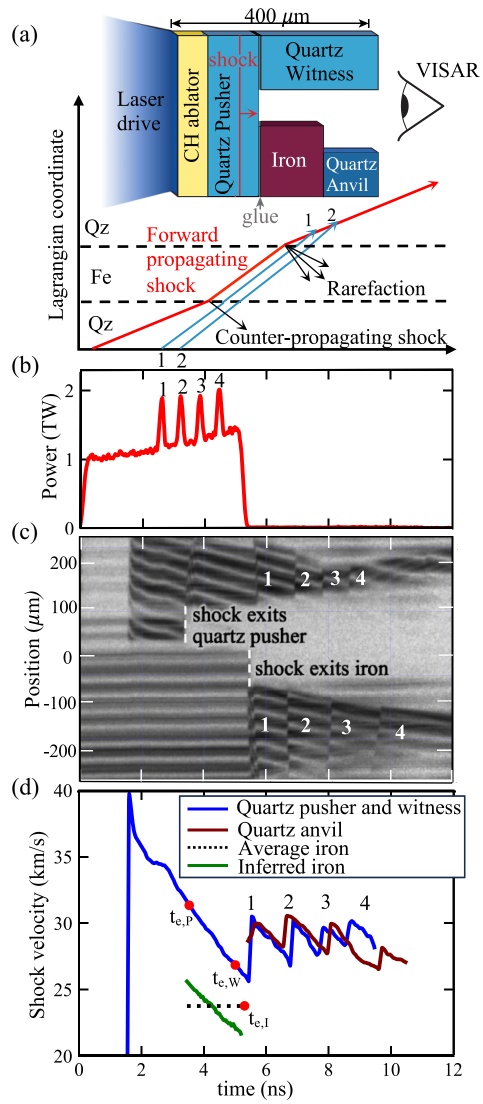

FIG. 1. (a) Schematic of the shock wave (red) and perturbations (blue) propagating through the target (inset). (b) An example of the laser pulse shape having four pickets separated by 200 ps that drive perturbations through the target. (c) VISAR interferometer fringes streaked in time where the upper and lower halves of the image show fringe movement due to changes in the shock velocity in the pusher and witness stack, and in the anvil, respectively. (d) Shock velocity histories extracted using Fourier analysis of the fringe displacements. The perturbation arrival times in the anvil compared to those in the witness provide a relative measure of sound speed between the iron and the quartz.

which is uniquely equipped to study the sound velocity on the primary Hugoniot because the perturbations can be tracked from their origins and correlated in time. The target, depicted in Fig. 1(a), was uniformly irradiated on one side by the high-power OMEGA EP laser, launching a 0.5–3 TPa shock wave. The OMEGA EP [46] facility's capability to precisely control the laser power allows the user to superimpose pickets onto the pulse shape which launch acoustic perturbations with an accuracy of 0.03 ns in time. The acoustic perturbations travel at the sound speed of the warm dense iron until they catch up to the initial leading shock wave. VISAR [47] (Velocity Interferometer System for Any Reflector) is used to measure the arrival times of the perturbations, which determine the sound speed of the material on the primary Hugoniot. α quartz serves as a reference material because it has a well known EOS and is reflective under shock compression [48–52]. Because iron is opaque to the 532 nm VISAR probe laser, the shock front velocity cannot be tracked directly inside the sample, as in previous works [32,33]. The shock front, however, is visible and tracked after it breaks out of the iron and into the quartz anvil [Fig. 1(c)]. The nonsteady waves correction [53] is applied to the shock velocity history in opaque iron [Fig. 1(d)] to determine the time-dependent deviations from the average shock velocity, using shock transit times measured with VISAR and the iron thicknesses (nominally 50 μm). The nominal quartz pusher thickness is 50 μm and the quartz anvil and witness are typically thicker than 150 μm.

III. ANALYSIS AND RESULTS

A. Nonsteady waves correction

The nonsteady waves correction [53] is a method to reconstruct the shock velocity history in the iron sample using the simultaneous shock velocity history in the quartz. The shock velocity in the iron is defined as

$$U_s^I(t) = \langle U_s^I \rangle + \delta U_s^I(t), \tag{1}$$

where $\langle U_s^I \rangle$ is the measured average shock velocity in iron, and $\delta U_s^I(t)$ is the time dependent deviation from that average. The deviations are determined using

$$\delta U_s^I(t) = G^I \delta U_s^W((t - t_{e,P})/F^I), \tag{2}$$

where F^I and G^I are linear scaling parameters relating the time dilation and amplitude, respectively, between the deviations from the average shock velocities in iron (I) and the quartz witness (W). A more physical interpretation of F^I is provided by considering Eq. (2) with Fig. 1(d). F^I describes the relative stretching or compression of the time axis to map the events in the iron sample to the same events in the quartz witness. For the experiment shown, the sound speed in quartz is higher than that of iron, so the acoustic perturbations spend more time in iron ($t_{e,I} - t_{e,P}$) than in quartz ($t_{e,W} - t_{e,P}$) and $F^I > 1$. The scaling parameter F^I is determined using Eqs. (3)–(5) below:

$$F^I = \frac{t_{e,I} - t_{e,P}}{t_{e,W} - t_{e,P}}, \tag{3}$$

where $t_{e,I}$ and $t_{e,P}$ are the times that the shock wave exits the iron and the quartz pusher, respectively. $t_{e,W}$ is an unknown that can be determined using the perturbation arrival times in the witness and the anvil (A). It is defined as

$$t_{e,W} = -F^A(t_{1,A} - t_{e,I}) + t_{1,W}, \tag{4}$$

where F^A is the linear scaling factor between the temporal perturbations in the witness and the anvil, and $t_{1,W}$ and $t_{1,A}$ are the times that the first perturbation (stemming from the laser pickets) catch up to the initial shock wave in the quartz witness and the quartz anvil, respectively. See Figs. 1(d) and

TABLE I. Measured and extracted quantities for the eight shots in this work, with uncertainties in parentheses. The average shock velocity in iron is calculated from the sample thickness, shock transit time, and glue thicknesses using $< U_{s,\mathrm{Fe}} >= \frac{\Delta x_{\mathrm{iron}}}{t_{\mathrm{transit}} - \Delta x_{\mathrm{glue}}/U_{s,\mathrm{glue}}}$, where $U_{s,\mathrm{glue}}$ was estimated from SESAME 7603 for epoxy [71]. Shot Nos. 26633 and 27180 were only used for Hugoniot measurements, as they did not have unambiguous perturbations in the shock velocity to reference. A value of 1.0 was used for F in these shots, which is described as the "zeroth order" correction in Ref. [53]. Glue thicknesses for shots 80114, 80116, and 26633 were not available; the average shock velocity was calculated assuming a glue thickness of 2.3 ± 1.9 μm (the nominal value being the average of the glue thickness measurements for shot Nos. 31383, 27722, 29766, 27180, 27443, 33718, and 31381, and the uncertainty being the standard deviation of those measurements). *Shots 80114 and 80116 report a combination iron and glue thickness (see Ref. [54]).

Shot No.	Δx_{iron} (μm)	t_{transit} (ns)	Δx_{glue} (μm)	$U_{s,\mathrm{glue}}$ (km/s)	$U_{s,\mathrm{Qz}}$ (km/s)	$< U_{s,\mathrm{Fe}} >$ (km/s)	F
80114	50.6 (0.7)*	4.33 (0.08)	2.3 (1.9)	16.0	14.4 (0.2)	11.5 (0.3)	0.9214 (0.0015)
80116	61.0 (1.7)*	4.66 (0.11)	2.3 (1.9)	16.1	14.5 (0.3)	13.0 (0.5)	1.0122 (0.0003)
31383	50.6 (1.3)	3.65 (0.01)	4.8 (2.1)	20.7	19.1 (0.2)	14.8 (0.6)	1.0629 (0.0014)
27722	50.1 (0.4)	3.21 (0.01)	0.4 (1.0)	20.6	18.5 (0.3)	15.7 (0.3)	1.0055 (0.0017)
26633	52.7 (1.2)	2.94 (0.03)	2.3 (1.9)	27.2	24.0 (0.2)	18.4 (0.4)	1.0 (N/A)
29766	54.4 (1.2)	2.67 (0.01)	1.1 (3.4)	27.3	24.1 (0.3)	20.7 (1.1)	0.9752 (0.0007)
27180	45.7 (0.7)	2.24 (0.06)	1.7 (1.9)	31.3	27.3 (0.2)	20.9 (0.9)	1.0 (N/A)
27443	45.2 (0.5)	2.01 (0.04)	2.2 (3.9)	35.2	30.4 (0.3)	23.2 (1.4)	0.9744 (0.0007)
33718	50.0 (2.0)	2.13 (0.01)	0.7 (2.3)	35.6	31.6 (0.3)	23.8 (1.2)	0.9415 (0.0010)
31381	50.1 (1.3)	2.17 (0.05)	5.1 (1.4)	40.2	34.7 (0.4)	24.5 (0.8)	0.8982 (0.0018)

S 2 of Ref. [54] for an illustration. F^{A}, G^{A}, and C are scaled using:

$$\delta U_{\mathrm{s}}^{\mathrm{A}}(t - t_{\mathrm{e,I}}) = G^{\mathrm{A}} * \delta U_{\mathrm{s}}^{\mathrm{W}}((t - t_{\mathrm{e,W}})/F^{\mathrm{A}}) + C \tag{5}$$

until the witness perturbations to the shock velocity are best fit to those in the anvil using a least squares minimization routine. G^{A} is the scaling parameter that accounts for amplitude variations in the velocity history. C is a free parameter which allows for a small (∼2%) vertical shift to remove any systematic offset between the anvil and witness perturbations. The least squares minimization returns an optimized F^A, which along with Eqs. (3) and (4), yields F^{I}. See Table I for values of F^{I}, along with other measured and extracted quantities.

The G^I parameter can be defined following the analysis in Ref. [53] as

$$G^{\mathrm{I}} = \frac{\delta u_I}{\delta u_W}, \tag{6}$$

where δu_I is the amplitude scaling factor for the side of the target with the iron sample, and δu_W is the amplitude scaling factor for the side of the target with only quartz (the witness side). For the amplitude scaling parameters, it is helpful to define the Mach number: $M_{\mathrm{Shock}} = \frac{u_f}{c_s}$, which is associated with a wave front (e.g., shock); u_f is the wave front velocity. It is also useful to define a quantity for compression: $\eta = \frac{\rho}{\rho_0}$. Following the analysis in Ref. [53], the equations for δu_I and δu_W can be written:

$$\begin{aligned}\delta u_I = M_{SP,d}&\frac{(M_{RP,u}+1)\big(1+M_{RP,u}^{-1}-(\eta_{SP,d}-1)M_{SP,d}^2\gamma_{SP,d}\big)}{(M_{RP,d}+1)\big(1+M_{SP,u}-(\eta_{SP,d}-1)M_{SP,d}^2\gamma_{SP,d}\big)}\\ &\times\frac{-2\eta_{SI,d}(M_{SI,d}-1)}{(\eta_{SI,d}-1)\big(1+M_{SI,d}-(\eta_{SI,d}-1)M_{SI,d}^2\gamma_{SI,d}\big)}\\ &\times\frac{2\rho_{RP,d}c_{RP,d}}{\rho_{SI,d}c_{SI,d}+\rho_{RP,d}c_{RP,d}}\end{aligned} \tag{7}$$

and

$$\delta u_W = \frac{-2\eta_{SW,d}(M_{SW,d}-1)}{(\eta_{SW,d}-1)\big(1+M_{SW,d}-(\eta_{SW,d}-1)M_{SW,d}^2\gamma_{SW,d}\big)}, \tag{8}$$

where the Mach numbers can be identified by the wave front they are associated with (S for shock, R for reshock or counter-propagating shock), and the region that event is in (P for pusher, W for witness, and I for iron), as well as whether the region is upstream or downstream of the shock event (u or d) [53]. In Eqs. (7) and (8), γ is the Grüneisen parameter for the region, identified the same way as the Mach number. For quartz, a constant value of 0.66 was used for γ, following the convention in Ref. [55].

To calculate the time-dependent shock velocity to be used in the Hugoniot determination, the witness and anvil scaling parameters (F^{A} and G^{A}) are first calculated using a least-squares minimization [Eq. (5)]. This determines F^I, and then G^I can be calculated. Because the G^I can be seen to depend on the Grüneisen parameter and Mach number for shocked iron, which are calculated using the sound speed, it is evident that this process will need an a priori assumption for sound speed and Grüneisen parameter and then will iterate to achieve convergence. The initial sound speed and Grüneisen parameter are taken from LEOS 260 (LEOS stands for Livermore equation of state, see Ref. [24]) at the measured shock velocity. Section III B describes how to calculate sound speed (also using F_I), so the calculated sound speed value will inform the next iteration of the calculation for the time dependent shock velocity. This time dependent shock velocity in iron is used to obtain the Hugoniot state via impedance matching [56] to the quartz standard (see Fig. S4 [54]). The process of obtaining the time-dependent shock velocity and calculating sound speed is repeated until G^I converges. The difference between the time-dependent shock velocity at the impedance match point between the initial guess and the iterated upon amplitude scaling factor is usually ∼1%, and the parameters typically converge in approximately three iterations. The Hugoniot data

TABLE II. Hugoniot data for iron obtained from the impedance-matching technique, which was determined at the time of breakout from the quartz pusher into the iron sample.

Shot No.	P (GPa)	ρ (g/cc)	$U_{s,\mathrm{Fe}}$ (km/s)	$U_{p,\mathrm{Fe}}$ (km/s)
80114	498 (12)	15.28 (0.50)	11.43 (0.21)	5.54 (0.13)
80116	530 (14)	13.75 (0.48)	12.55 (0.35)	5.36 (0.14)
31383	952 (17)	16.63 (0.78)	15.15 (0.42)	7.98 (0.13)
27722	927 (17)	14.72 (0.33)	15.91 (0.21)	7.40 (0.13)
26633	1614 (29)	18.89 (0.93)	18.75 (0.42)	10.93 (0.18)
29766	1694 (42)	16.70 (1.10)	20.20 (0.78)	10.65 (0.23)
27180	2283 (43)	16.90 (0.79)	23.30 (0.64)	12.44 (0.21)
27443	2773 (76)	21.20 (2.20)	23.65 (0.99)	14.89 (0.34)
33718	3116 (72)	18.60 (1.20)	26.20 (0.85)	15.11 (0.31)
31381	3708 (77)	22.20 (1.40)	27.00 (0.57)	17.44 (0.33)

obtained in this work (see Table II) can then be fit along with previous experimental Hugoniot data and the fit is used in the calculation of sound speed and Grüneisen parameter, described in Sec. III B. A piecewise orthogonal basis linear fit was performed in $U_\mathrm{s} - U_\mathrm{p}$ as outlined in Ref. [57]. The fit takes the form $U_s = c_0 + SU_p$. The breakpoint in the Hugoniot fit was found to be $U_p \simeq 6.0$ km/s. For the fit to the data below $U_p \simeq 6.0$ km/s (but above the liquid transition around $U_p \simeq 3.8$ km/s), $c_0 = 4.54 \pm 0.05$ and $S = 1.46 \pm 0.03$. For the fit above $U_p \simeq 6.0$ km/s, $c_0 = 5.82 \pm 0.06$ and $S = 1.26 \pm 0.02$. The data and fit are shown in Figs. 2 and 3.

B. Lagrangian sound speed calculation

Using the scaling parameter F^I, determined above, and the formalism described in Ref. [53], an expression is assembled for the sound speed (c_s) in iron on the primary Hugoniot, which depends on the scaling parameter F^I, pressure (P), density (ρ), particle velocity (U_p), and Mach numbers for the shocked quartz and reshocked quartz:

$$c_s^{SI,d} = \frac{P^{SI,d}}{U_p^{SI,d}\rho^{SI,d}}\left[1 - \frac{1 - M_{SW,d}}{F^I}\frac{1 + M_{RP,u}}{1 + M_{RP,d}}\right]^{-1}, \quad (9)$$

where the Mach numbers and subscripts follow the same convention used in Eqs. (7) and (8). Because the laser-induced perturbations are affected by the time-dependent pressure fluctuations caused by the nonsteady shock wave as they transit the entirety of the iron, the sound speed determination happens over a locus of pressure states rather than one single state. Therefore the Hugoniot state associated with the sound speed measurement is averaged over the time dependent velocity, rather than using the Hugoniot state at the impedance matching boundary for that specific shot. The density used to calculate the sound speed was inferred from the bilinear fit to all existing Hugoniot data, rather than an individual impedance matching measurement.

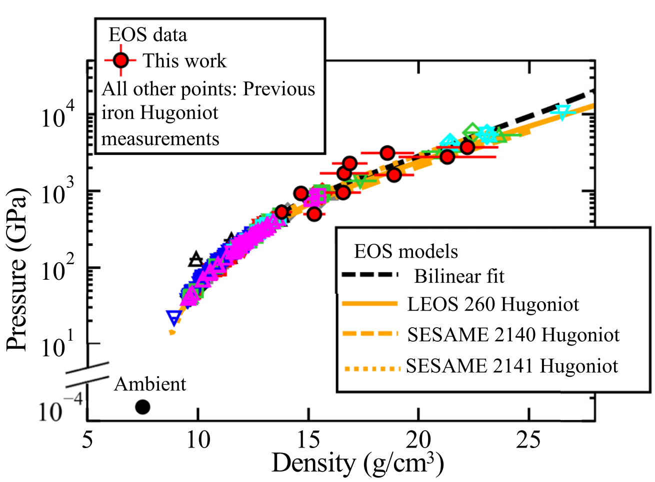

FIG. 2. Iron Hugoniot data from this work and references [12–18,22,58–70], the bilinear $U_s - U_p$ Hugoniot fit, and Hugoniots from the EOS tables [24–26] are shown in the shock pressure-density plane. Each dataset from the references uses a unique color and marker shape combination. The ambient pressure and density (7.875 g/cm^3) of iron is shown as a filled black circle.

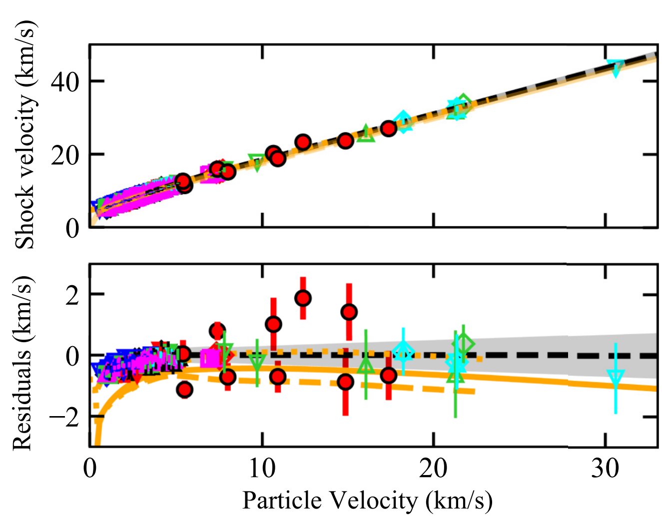

FIG. 3. Hugoniot data from this work and references [12–18,22,58–70], the bilinear $U_\mathrm{s} - U_\mathrm{p}$ Hugoniot fit, and Hugoniots from the EOS tables [24–26] are shown in the shock velocity-particle velocity plane. The breakpoint for the bilinear fit is at $U_\mathrm{p} = 6.0$ km/s. The lower plot shows the residuals for the bilinear fit compared to the tabular EOS. The legend for this figure is the same as shown in Fig. 2.

TABLE III. Sound speed and Grüneisen parameter in shocked iron, with uncertainties in parentheses. The pressure and density are calculated using the measured average shock speed in Table I and the iron Hugoniot fit described in the text. The average values here differ from the corresponding Hugoniot measurements for the same shots reported in Table II due to the variation in the strength as the shock transits the iron layer.

Shot No.	$< P >$ (GPa)	$< \rho >$ (g/cc)	C_s (km/s)	γ
80114	432 (31)	13.5 (0.3)	10.9 (0.4)	1.33 (0.16)
80116	594 (59)	14.2 (0.3)	12.4 (0.5)	1.19 (0.14)
31383	833 (91)	15.2 (0.4)	12.7 (0.5)	0.93 (0.14)
27722	972 (51)	15.8 (0.3)	13.4 (0.5)	0.86 (0.11)
29766	1930 (250)	18.4 (0.6)	15.3 (0.6)	0.91 (0.06)
27443	2530 (360)	19.5 (0.7)	17.0 (0.7)	0.84 (0.06)
33718	2680 (320)	19.8 (0.7)	16.8 (0.7)	0.87 (0.05)
31381	2870 (220)	20.0 (0.6)	16.7 (0.7)	0.89 (0.05)

In this way, the sound speed can be accurately determined despite a nonsteady shock wave transiting the iron region. For the data in this work, iron was fully melted, and therefore its strength can be neglected [72]. The assumption is made that the first pressure perturbation reaches the shock front at a point in time very close to the when the shock front exits the iron, which ensures that perturbation will have only traveled through a small amount (<30 %) of released iron.

C. Grüneisen parameter calculation

Using the sound speed measurement for iron, the iron Grüneisen parameter on the Hugoniot is calculated using the equation introduced in Ref. [73]:

$$\gamma = \frac{-c_s^2 + \frac{dP}{d\rho}\big|_H}{-\frac{1}{2}\frac{P}{\rho} + \frac{\rho}{2}\frac{dP}{d\rho}\big|_H\left(\frac{1}{\rho_0} - \frac{1}{\rho}\right)}, \tag{10}$$

where ρ_0 is the ambient density of iron and the subscript "H" denotes that a quantity lies on the Hugoniot.

D. Uncertainty analysis

Systematic uncertainty analysis for this work incorporates measurements of target component thickness, glue thickness, and determination of transit times time ($t_{e,I}$, $t_{e,P}$) in the impedance matching calculation. As these data were collected over a long period of time, individual shots with larger error bars in this data can be attributed to difference in experimental setup and initial metrology. An uncertainty of 3% of the sound speed value was also added in quadrature to the other sources of error, as this was how closely the analysis method described in this work reproduced values from simulations (see Ref. [54] for more information). Uncertainties in the Grüneisen parameter are calculated from the Hugoniot fit to $U_s - U_p$ (Fig. 3) and the uncertainty on the individual sound speed measurements (Table III). Notably, the uncertainty on the Grüneisen parameter is lowered with increased pressure. This is because the expression used for the Grüneisen parameter convolves the slope of the Hugoniot, the $U_s - U_p$ fit, and the reference EOS for alpha-quartz [74], which produces a systematic decrease in the uncertainty on Grüneisen parameter at high pressures and densities. A Monte Carlo approach was used to propagate uncertainties through the calculations.

IV. RESULTS

The sound speed measurements of iron to 20 g/cm^3 and 3 TPa obtained in this work are presented in Fig. 4 with those from previous experimental works [12,16,16,17,36] and tabular equations of state [24,25]. These data demonstrate that the sound speed of iron on the Hugoniot is very close to the sound speed of iron on a quasi-isentropic compression path at the same densities [11], despite the increased temperature produced during shock compression. The data in this work are systematically lower than an extrapolation to the previous highest density sound speed measurement on the Hugoniot by Sakaiya, *et al.* [36].

Eight discreet Grüneisen parameter values were determined from Eq. (10) using the Hugoniot and sound speed data from this work (Fig. 5) at pressures between ∼450 and 3000 GPa and densities between ∼13.5 and 20 g/cm^3 along the Hugoniot. Using LEOS 260 [24] to estimate temperatures from our measured pressures suggests these Grüneisen parameter values range from approximately 6000 to 80 000 K. These data compare well to values on the Hugoniot calculated here in the same manner from the sound speeds reported in Refs. [17] and [16] at pressures of ∼250–400 GPa and densities of ∼12.2–13.2 g/cm^3, as well as measurements of the vibrational Grüneisen parameter in solid HCP iron at 300 K [29,30] (Fig. 5). These data sets for different thermodynamic paths suggest a strong dependence of the Grüneisen parameter on temperature and phase. The Grüneisen parameter for the isentrope and Hugoniot from the EOS tables diverge at densities (and temperatures) above where the Hugoniot crosses the melt. That is, the Hugoniot temperature increases more rapidly with pressure than the isentrope, and crosses the melt curve at 220–260 GPa, and 12.1–12.3 g/cm^3, while iron on the isentrope (starting from STP conditions) remains solid. Commonly used models for the Grüneisen parameter [75,76] assume temperature independence and a linear or exponential dependence on volume, so these models do not capture the behavior exhibited in Fig. 5. A similar change in Grüneisen parameter in the vicinity of melt is also observed in Mg_2SiO_4 [77]. Other materials in the literature (aluminum [40] and periclase [78]) show possible signs of melt and temperature dependence in Grüneisen parameter, but cannot be investigated further without more data.

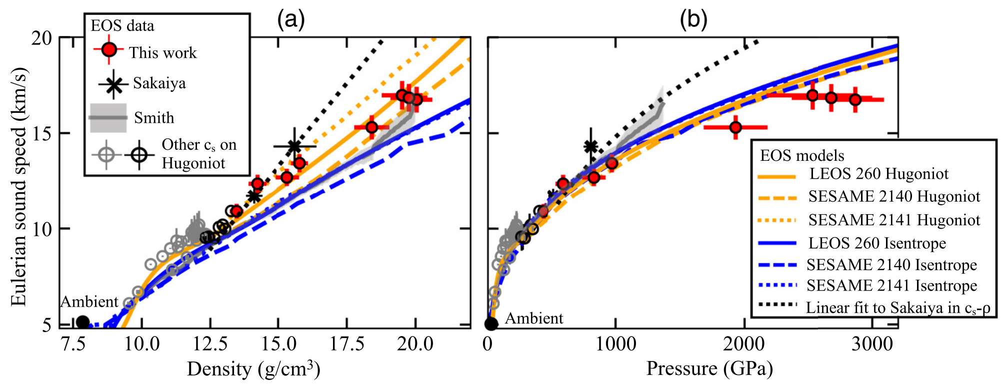

FIG. 4. Iron sound speed vs (a) density and (b) pressure. The data collected in this work is shown in red. Other sound speed measurements on the Hugoniot by Brown and McQueen, Altshuler, and Nguyen and Holmes [12,16,17,36] are shown with the open grey and black circles. Black denotes fluid measurements and grey denotes solid measurements. The Smith, *et al*, data can be characterized as an average value between the isentrope and the Hugoniot [11]. The linear fit to the Sakaiya, *et al.* data [36] was done in the density-sound speed plane and then translated to the pressure-sound speed plane using a $U_s - U_p$ fit to the Hugoniot data. Tabular EOS predictions [24–26] are shown as blue (isentropic) and orange (Hugoniot) lines.

Three tabular equations of state were selected to compare to this letter's measurements of sound speed and Grüneisen parameter. SESAME 2140 (SESAME is the library of the Los Alamos National Laboratory equations of state, see Ref. [79]) calculates the cold curve, ionic contribution, and electronic contribution separately. The fluid, high pressure and temperature phase is calculated using the Cowan model for ions and Thomas-Fermi-Dirac (TFD) for the electron contribution. LEOS 260 [24] uses a quotidian equation of state, also based on the Thomas-Fermi theory for the electrons and a Cowan model connecting the solid state and fluid state for the ions, albeit adjusting for experimental data [80]. SESAME 2141 [26] is a five-phase EOS table based on quantum molecular dynamics calculations and experimental data.

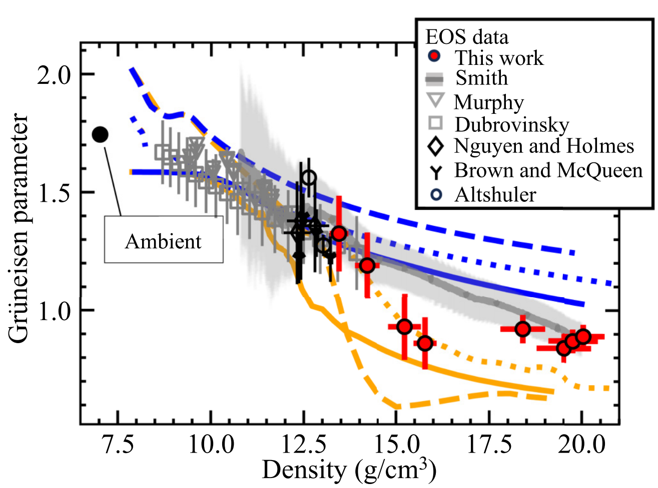

FIG. 5. Iron Grüneisen parameter extracted using Eq. (10) (red closed circles). Black open points denote fluid measurements and grey open points denote solid measurements [16,17,29,30,36,61]. The Grüneisen parameter data for Refs. [16,17,36,61] were calculated using Eq. (10). The measurement of ambient pressure, fluid Grüneisen parameter by Anderson [4] is liquid at 1811 K. The blue and orange curves are the SESAME and LEOS tabular equations of state, which follow the same legend as Fig. 4.

The new data presented here are at warm dense matter conditions, which are particularly difficult to model. The experimentally determined Hugoniot (Figs. 2 and 3) agrees best with SESAME 2141. At TPa pressures, both LEOS 260 and SESAME 2140 over-predict compression (at P = 2000 GPa, $(\rho_{\text{data}} - \rho_{\text{model}})/\rho_{\text{data}} \sim 3\%$ and 6%, respectively). The sound speed as a function of pressure is not well represented by any of the tabular equations of state, stemming in part from this systematic difference between the experimental Hugoniot fit and the tabular models. In density space, the sound speed best matches the prediction by LEOS 260, but the Grüneisen parameter is best represented by SESAME 2141. The inability of a single theoretical method (quantum molecular dynamics or classical TFD) to match both derivatives of the equation of state highlights a breakdown in our theoretical understanding for iron in the warm dense matter regime. While the specific construction methods of compression, sound speed, and Grüneisen parameter vary across tabular equations of state, the complex relationship of ion and electron structures can often lead to compensating errors and systematic offsets. The measurements of the derivatives of the equation of state in this work provide theorists with a more sensitive constraint in the terapascal pressure range.

In summary, the iron principal Hugoniot, sound speed, and Grüneisen parameter were measured to 3 TPa. These measurements extend the experimental dataset for the sound speed and Grüneisen parameter on the Hugoniot by a factor of ∼6. Investigating these key derivatives reveals relationships that cannot be extracted from the pressure-density equation of state alone. The sound speed changes relatively little as the temperature difference between the Hugoniot and the isentrope grows, which implies a smaller resistance to shock compression than previously predicted. The Grüneisen parameter's slow decline with increasing density and sudden drop after the melt transition on the Hugoniot demonstrates the dependence of pressure on thermal energy from shock heating and on restructuring of atoms upon melt. While there are theoretical equations of state that can roughly predict either the sound speed or the

Grüneisen data in iron, none of the current models can self-consistently explain the two. This work and previous works are just starting to investigate what the Grüneisen parameter can tell us about high energy density matter, and follow-up studies on other materials are necessary to probe the behavior in this regime.

ACKNOWLEDGMENTS

The authors thank Dr. Marius Millot, Dr. Jon Eggert, Dr. Peter Celliers, and Dr. Richard Kraus from LLNL for helpful discussions. The authors also wish to thank Felipe Gonzalez-Cataldo (U.C. Berkeley) for discussion of the Grüneisen parameter. The VISAR data were analyzed using the LLNL Analyze VISAR code. This material is based upon work supported by the Department of Energy National Nuclear Security Administration under Award No. DE-NA0003856, the University of Rochester, and the New York State Energy Research and Development Authority. (M.F.H., M.C.M., B.J.H., X.G., T.S., E.A.S., J.R.R., G.W.C.) Part of this work was performed under the auspices of the U.S. Department of Energy by Lawrence Livermore National Laboratory under contract DE-AC52-07NA27344. (D.E.F.) Sandia National Laboratories is supported by the U.S. Department of Energys National Nuclear Security Administration under Contract No. DE-NA0003525. (C.A.M.) Funding for this research was provided by the Center for Matter at Atomic Pressures (CMAP), a National Science Foundation (NSF) Physics Frontiers Center, under Award PHY2020249.

This report was prepared as an account of work sponsored by an agency of the U.S. Government. Neither the U.S. Government nor any agency thereof, nor any of their employees, makes any warranty, express or implied, or assumes any legal liability or responsibility for the accuracy, completeness, or usefulness of any information, apparatus, product, or process disclosed, or represents that its use would not infringe privately owned rights. Reference herein to any specific commercial product, process, or service by trade name, trademark, manufacturer, or otherwise does not necessarily constitute or imply its endorsement, recommendation, or favoring by the U.S. Government or any agency thereof. The views and opinions of authors expressed herein do not necessarily state or reflect those of the U.S. Government or any agency thereof.

[1] S. Stewart, E. Davies, M. Duncan, S. Lock, S. Root, J. Townsend, R. Kraus, R. Caracas, and S. Jacobsen, The shock physics of giant impacts: Key requirements for the equations of state, AIP Conf. Proc. **2272**, 080003 (2020).

[2] N. Hosono and S.-i. Karato, The influence of equation of state on the giant impact simulations, J. Geophys. Res.: Planets **127**, e2021JE006971 (2022).

[3] R. G. Kraus, S. Root, R. W. Lemke, S. T. Stewart, S. B. Jacobsen, and T. R. Mattsson, Impact vaporization of planetesimal cores in the late stages of planet formation, Nature Geoscience **8**, 269 (2015).

[4] W. W. Anderson and T. J. Ahrens, An equation of state for liquid iron and implications for the earth's core, J. Geophys. Res.: Solid Earth **99**, 4273 (1994).

[5] S. C. Grant, T. Ao, C. T. Seagle, A. J. Porwitzky, J.-P. Davis, K. R. Cochrane, D. H. Dolan, J.-F. Lin, T. Ditmire, and A. C. Bernstein, Equation of state measurements on iron near the melting curve at planetary core conditions by shock and ramp compressions, J. Geophys. Res.: Solid Earth **126**, e2020JB020008 (2021).

[6] B. A. Buffett, Earth's core and the geodynamo, Science **288**, 2007 (2000).

[7] S.-F. Liu, Y. Hori, S. Müller, X. Zheng, R. Helled, D. Lin, and A. Isella, The formation of jupiter's diluted core by a giant impact, Nature (London) **572**, 355 (2019).

[8] G. W. Marcy, L. M. Weiss, E. A. Petigura, H. Isaacson, A. W. Howard, and L. A. Buchhave, Occurrence and core-envelope structure of $1-4\times$ earth-size planets around sun-like stars, Proc. Natl. Acad. Sci. USA **111**, 12655 (2014).

[9] R. Helled, D. J. Stevenson, J. I. Lunine, S. J. Bolton, N. Nettelmann, S. Atreya, T. Guillot, B. Militzer, Y. Miguel, and W. B. Hubbard, Revelations on jupiter's formation, evolution and interior: Challenges from juno results, Icarus **378**, 114937 (2022).

[10] R. G. Kraus, R. J. Hemley, S. J. Ali, J. L. Belof, L. X. Benedict, J. Bernier, D. Braun, R. E. Cohen, G. W. Collins, F. Coppari, M. P. Desjarlais, D. Fratanduono, S. Hamel, A. Krygier, A. Lazicki, J. Mcnaney, M. Millot, P. C. Myint, M. G. Newman, J. R. Rygg *et al.*, Measuring the melting curve of iron at super-earth core conditions, Science **375**, 202 (2022).

[11] R. Smith, D. Fratanduono, and D. Braun, Equation of state of iron under core conditions of large rocky exoplanets, Nature Astronomy **2**, 452458 (2018).

[12] L. V. Al'tshuler, R. F. Trunin, K. K. Krupnikov, and N. V. Panov, Explosive laboratory devices for shock wave compression studies, Phys. Usp. **39**, 539 (1996).

[13] R. F. Trunin, M. A. Podurets, L. V. Popov, V. N. Zubarev, A. A. Bakanova, V. M. Ktitorov, A. G. Sevast'yanov, G. V. Simakov, and I. P. Dudoladov, Measurement of the compressibility of iron at 5.5 TPa, Zh. Eksp. Teor. Fiz. **102**, 1433 (1992) [Sov. Phys. JETP **75**, 777 (1992)].

[14] R. F Trunin, M. A. Podurets, L. V. Popov, B. N. Moiseev, G. V. Simakov, and A. G. Sevast'yanov, Determination of the shock compressibility of iron at pressures up to 10 Tpa (100 Mbar), Zh. Eksp. Teor. Fiz. **103**, 2189 (1993) [Sov. Phys. JETP **76**, 1095 (1993)].

[15] R. F. Trunin, Shock compressibility of condensed materials in strong shock waves generated by underground nuclear explosions, Phys. Usp. **37**, 1123 (1994).

[16] J. M. Brown and R. G. Mcqueen, Phase transitions, gruneisen parameter, and elasticity for shocked iron between 77 Gpa and 400 Gpa, J. Geophys. Res.: Solid Earth **91**, 7485 (1986).

[17] J. H. Nguyen and N. C. Holmes, Melting of iron at the physical conditions of the earths core, Nature (London) **427**, 339 (2004).

[18] K. K. Krupnikov, A. A. Bakanova, M. I. Brazhnik, and R. F. Trunin, An investigation of the shock compressibility of Ti-

tanium, Molybdenum Tantalum, and Iron, Dokl. Akad. Nauk SSSR **148**, 1302 (1963) [Sov. Phys. Dokl. **8**, 205 (1963)].

[19] D. Batani, A. Morelli, M. Tomasini, A. Benuzzi-Mounaix, F. Philippe, M. Koenig, B. Marchet, I. Masclet, M. Rabec, C. Reverdin, R. Cauble, P. Celliers, G. Collins, L. Da Silva, T. Hall, M. Moret, B. Sacchi, P. Baclet, and B. Cathala, Equation of state data for iron at pressures beyond 10 Mbar, Phys. Rev. Lett. **88**, 235502 (2002).

[20] Y. Ping, F. Coppari, D. G. Hicks, B. Yaakobi, D. E. Fratanduono, S. Hamel, J. H. Eggert, J. R. Rygg, R. F. Smith, D. C. Swift, D. G. Braun, T. R. Boehly, and G. W. Collins, Solid iron compressed up to 560 Gpa, Phys. Rev. Lett. **111**, 065501 (2013).

[21] J. Wang, R. F. Smith, J. H. Eggert, D. G. Braun, T. R. Boehly, J. Reed Patterson, P. M. Celliers, R. Jeanloz, G. W. Collins, and T. S. Duffy, Ramp compression of iron to 273 Gpa, J. Appl. Phys. **114**, 023513 (2013).

[22] C. E. Ragan, Shock-wave experiments at threefold compression, Phys. Rev. A **29**, 1391 (1984).

[23] R. Wissing and D. Hobbs, A new equation of state applied to planetary impacts - i. models of planetary interiors, A&A **635**, A21 (2020).

[24] H. D. Whitley and P. A. Sterne, Report No. LLNL-TR-812823 (Lawrence Livermore National Laboratory, Livermore, CA, 2020).

[25] S. P. Lyon and J. D. Johnson, Report No. LA-UR-3407 (Los Alamos National Laboratory, Los Alamos, NM, 1992).

[26] T. Sjostrom and S. Crockett, Quantum molecular dynamics of warm dense iron and a five-phase equation of state, Phys. Rev. E **97**, 053209 (2018).

[27] H. Ichikawa, T. Tsuchiya, and Y. Tange, The p-v-t equation of state and thermodynamic properties of liquid iron, J. Geophys. Res.: Solid Earth **119**, 240 (2014).

[28] P. I. Dorogokupets, A. M. Dymshits, K. D. Litasov, and T. S. Sokolova, Thermodynamics and equations of state of iron to 350 Gpa and 6000 K, Sci. Rep. **7**, 41863 (2017).

[29] L. S. Dubrovinsky, N. A. Dubrovinskaia, and T. Le Bihan, Aggregate sound velocities and acoustic grüneisen parameter of iron up to 300 Gpa and 1,200 K, Proc. Natl. Acad. Sci. USA **98**, 9484 (2001).

[30] C. A. Murphy, J. M. Jackson, W. Sturhahn, and B. Chen, Gruneisen parameter of hcp-Fe to 171 Gpa, Geophys. Res. Lett. **38**, L24306 (2011).

[31] D. E. Fratanduono, P. M. Celliers, D. G. Braun, P. A. Sterne, S. Hamel, A. Shamp, E. Zurek, K. J. Wu, A. E. Lazicki, M. Millot, and G. W. Collins, Equation of state, adiabatic sound speed, and Grüneisen coefficient of boron carbide along the principal Hugoniot to 700 Gpa, Phys. Rev. B **94**, 184107 (2016).

[32] D. E. Fratanduono, M. Millot, A. Fernandez Pañella, P. A. Sterne, G. W. Collins, D. G. Hicks, J. H. Eggert, T. R. Boehly, and P. M. Celliers, Measurement of the sound speed in dense fluid deuterium along the cryogenic liquid Hugoniot, Phys. Plasmas **26**, 012710 (2019).

[33] D. E. Fratanduono, M. Millot, R. G. Kraus, D. K. Spaulding, G. W. Collins, P. M. Celliers, and J. H. Eggert, Thermodynamic properties of $MgSiO_3$ at super-earth mantle conditions, Phys. Rev. B **97**, 214105 (2018).

[34] C. A. McCoy, M. D. Knudson, and M. P. Desjarlais, Sound velocity, shear modulus, and shock melting of beryllium along the Hugoniot, Phys. Rev. B **100**, 054107 (2019).

[35] C. A. McCoy, M. D. Knudson, and S. Root, Absolute measurement of the Hugoniot and sound velocity of liquid copper at multimegabar pressures, Phys. Rev. B **96**, 174109 (2017).

[36] T. Sakaiya, H. Takahashi, T. Kondo, T. Kadono, Y. Hironaka, T. Irifune, and K. Shigemori, Sound velocity and density measurements of liquid iron up to 800 Gpa: A universal relation between birch's law coefficients for solid and liquid metals, Earth Planet. Sci. Lett. **392**, 80 (2014).

[37] D. Antonangeli and E. Ohtani, Sound velocity of hcp-fe at high pressure: Experimental constraints, extrapolations and comparison with seismic models, Prog. in Earth and Planet. Sci. **2**, 3 (2015).

[38] R. Marcus, S. Stewart, D. Sasselov, and L. Hernquist, Collisional stripping and disruption of super-earths, Astrophys. J. **700**, L118 (2009).

[39] M. Nakajima, H. Genda, E. Asphaug, and S. Ida, Large planets may not form fractionally large moons, Nat. Commun. **13**, 568 (2022).

[40] T. S. Duffy and T. J. Ahrens, Sound velocities at high pressure and temperature and their geophysical implications, J. Geophys. Res.: Solid Earth **97**, 4503 (1992).

[41] G. H. Wolf and R. Jeanloz, Lindemann melting law: Anharmonic correction and test of its validity for minerals, J. Geophys. Res.: Solid Earth **89**, 7821 (1984).

[42] O. L. Anderson, The Grüneisen parameter for iron at outer core conditions and the resulting conductive heat and power in the core, Phys. Earth Planet. Inter. **109**, 179 (1998).

[43] F. D. Stacey and J. H. Hodgkinson, Thermodynamics with the Grüneisen parameter: Fundamentals and applications to high pressure physics and geophysics, Phys. Earth Planet. Inter. **286**, 42 (2019).

[44] M. C. Gregor, D. E. Fratanduono, C. A. McCoy, D. N. Polsin, A. Sorce, J. R. Rygg, G. W. Collins, T. Braun, P. M. Celliers, J. H. Eggert, D. D. Meyerhofer, and T. R. Boehly, Hugoniot and release measurements in diamond shocked up to 26 Mbar, Phys. Rev. B **95**, 144114 (2017).

[45] L. E. Crandall, J. R. Rygg, D. K. Spaulding, M. F. Huff, M. C. Marshall, D. N. Polsin, R. Jeanloz, T. R. Boehly, M. Zaghoo, B. J. Henderson, S. Brygoo, P. M. Celliers, J. H. Eggert, D. E. Fratanduono, A. Lazicki, M. Millot, and G. W. Collins, Equation-of-state, sound speed, and reshock of shock-compressed fluid carbon dioxide, Phys. Plasmas **28**, 022708 (2021).

[46] D. Meyerhofer, J. Bromage, C. Dorrer, J. Kelly, B. Kruschwitz, S. Loucks, R. Mccrory, S. Morse, J. Myatt, P. Nilson, J. Qiao, T. Sangster, C. Stoeckl, L. Waxer, and J. Zuegel, Performance of and initial results from the OMEGA EP laser system, J. Phys.: Conf. Ser. **244**, 032010 (2010).

[47] P. M. Celliers, D. K. Bradley, G. W. Collins, D. G. Hicks, T. R. Boehly, and W. J. Armstrong, Line-imaging velocimeter for shock diagnostics at the OMEGA laser facility, Rev. Sci. Instrum. **75**, 4916 (2004).

[48] D. G. Hicks, T. R. Boehly, J. H. Eggert, J. E. Miller, P. M. Celliers, and G. W. Collins, Dissociation of liquid silica at high pressures and temperatures, Phys. Rev. Lett. **97**, 025502 (2006).

[49] D. G. Hicks, T. R. Boehly, P. M. Celliers, J. H. Eggert, E. Vianello, D. D. Meyerhofer, and G. W. Collins, Shock compres-

sion of quartz in the high-pressure fluid regime, Phys. Plasmas **12**, 082702 (2005).

[50] M. P. Desjarlais, M. D. Knudson, and K. R. Cochrane, Extension of the Hugoniot and analytical release model of α-quartz to 0.2-3 TPa, J. Appl. Phys. **122**, 035903 (2017).

[51] T. Sjostrom and S. Crockett, A liquid regime equation of state for silicon dioxide, AIP Conf. Proc. **1793**, 050010 (2017).

[52] M. C. Marshall, A. E. Lazicki, D. Erskine, R. A. London, D. E. Fratanduono, P. M. Celliers, J. H. Eggert, F. Coppari, D. C. Swift, P. A. Sterne, H. D. Whitley, and J. Nilsen, Developing quartz and molybdenum as impedance-matching standards in the 100-Mbar regime, Phys. Rev. B **99**, 174101 (2019).

[53] D. E. Fratanduono, D. H. Munro, P. M. Celliers, and G. W. Collins, Hugoniot experiments with unsteady waves, J. Appl. Phys. **116**, 033517 (2014).

[54] See Supplemental Material at http://link.aps.org/supplemental/10.1103/PhysRevB.109.184311 for an analysis of simulated data using the HYADES hydrocode (Ref. [81]), a discussion of the impedance matching technique, and a discussion of the glue thickness calculation.

[55] S. Brygoo, M. Millot, P. Loubeyre, A. E. Lazicki, S. Hamel, T. Qi, P. M. Celliers, F. Coppari, J. H. Eggert, D. E. Fratanduono, D. G. Hicks, J. R. Rygg, R. F. Smith, D. C. Swift, G. W. Collins, and R. Jeanloz, Analysis of laser shock experiments on precompressed samples using a quartz reference and application to warm dense hydrogen and helium, J. Appl. Phys. **118**, 195901 (2015).

[56] M. A. Barrios, D. G. Hicks, T. R. Boehly, D. E. Fratanduono, J. H. Eggert, P. M. Celliers, G. W. Collins, and D. D. Meyerhofer, High-precision measurements of the equation of state of hydrocarbons at 10 Mbar using laser-driven shock waves, Phys. Plasmas **17**, 056307 (2010).

[57] P. M. Celliers, G. W. Collins, D. G. Hicks, and J. H. Eggert, Systematic uncertainties in shock-wave impedance-match analysis and the high-pressure equation of state of Al, J. Appl. Phys. **98**, 113529 (2005).

[58] I. C. Skidmore and E. Morris, in *Proceedings of the Symposium on Thermodynamics of Nuclear Materials* (IAEA, Vienna, 1962), p. 173.

[59] A. S. Balchan and G. R. Cowan, Shock compression of two iron-silicon alloys to 2.7 megabars, J. Geophys. Res. **71**, 3577 (1966).

[60] J. M. Walsh, M. H. Rice, R. G. McQueen, and F. L. Yarger, Shock-wave compressions of twenty-seven metals. equations of state of metals, Phys. Rev. **108**, 196 (1957).

[61] L. V. Al'tshuler, S. B. Kormer, M. I. Brazhnik, L. A. Vladimirov, M. P. Speranskaya, and A. I. Funtikov, The isentropic compressibilty of aluminum, copper, lead, and iron at high pressures, J. Exptl. Theor. Phys. (USSR) **38**, 1061 (1960) [Sov. Phys. JETP **11**, 766 (1960)].

[62] L. V. Al'tshuler, S. B. Kormer, A. A. Bakanova, and R. F. Trunin, Equation of state for aluminum, copper, and lead in the high-pressure region, J. Exptl. Theor. Phys. (USSR) **38**, 790 (1960) [Sov. Phys. JETP **11**, 573 (1960)].

[63] L. V. Al'tshuler, A. A. Bakanova, and R. F. Trunin, Shock adiabats and zero isotherms of seven metals at high pressures, J. Exptl. Theor. Phys. (USSR) **42**, 91 (1962) [Sov. Phys. JETP **15**, 65 (1962)].

[64] L. V. Altshuler, K. K. Krupnikov, B. N. Ledenev, V. I. Zhuchikhin, and M. I. Brazhnik, Dynamical compressibility and equation of state for iron under high pressure, Zh. Eksp. Teor. Fiz. **34**, 614 (1958).

[65] R. G. McQueen and S. P. Marsh, Equation of state for nineteen metallic elements from shock-wave measurements to two megabars, J. Appl. Phys. **31**, 1253 (1960).

[66] R. G. McQueen, S. P. Marsh, J. W. Taylor, J. N. Fritz, and J. W. Carter, The equation of state of solids from shock wave studies, in *High-Velocity Impact Phenomena*, edited by R. Kinslow (Academic Press, Cambridge, MA, 1970), pp. 293–417.

[67] R. S. Hixon and J. N. Fritz, Shock compression of iron, in *Shock Compression of Condensed Matter* (Elsevier Science Publishers, B.V., Amsterdam, the Netherlands, 1991).

[68] L. V. Al'tshuler and B. S. Chekin, in *Proceedings of the 1st All-Union Pulsed Pressures Symposium* (VNIIFTRI, 1974), pp. 5–22.

[69] L. V. Al'tshuler, N. N. Kalitkin, L. V. Kuz'mina, and B. S. Chekin, Shock adiabats for ultrahigh pressures, Zh. Eksp. Teor. Fiz. **72**, 317 (1977) [Sov. Phys. JETP **45**, 167 (1977)].

[70] L. V. Al'tshuler, A. A. Bakanova, I. P. Dudoladov, E. A. Dynin, R. F. Trunin, and B. S. Chekin, Shock adiabatic curves of metals, J. Appl. Mech. Tech. Phys. **22**, 145 (1981).

[71] J. C. Boettger, Report No. LA-12755-MS (Los Alamos National Laboratory, Los Alamos, NM, 1994).

[72] S. A. Thomas, M. C. Hawkins, M. K. Matthes, G. T. Gray, and R. S. Hixson, Dynamic strength properties and alpha-phase shock hugoniot of iron and steel, J. Appl. Phys. **123**, 175902 (2018).

[73] R. G. McQueen, S. P. Marsh, and J. N. Fritz, Hugoniot equation of state of twelve rocks, J. Geophys. Res. **72**, 4999 (1967).

[74] M. D. Knudson and M. P. Desjarlais, Shock compression of quartz to 1.6 Tpa: Redefining a pressure standard, Phys. Rev. Lett. **103**, 225501 (2009).

[75] J. Shanker, B. Singh, and H. Baghel, Volume dependence of the Grüneisen parameter and maximum compression limit for iron, Phys. B: Condens. Matter **387**, 409 (2007).

[76] L. V. Al'tshuler, S. E. Brusnikin, and E. A. Kuz'menkov, Isotherms and Grüneisen functions for 25 metals, J. Appl. Mech. Tech. Phys. **28**, 129 (1987).

[77] E. J. Davies, P. J. Carter, S. Root, R. G. Kraus, D. K. Spaulding, S. T. Stewart, and S. B. Jacobsen, Silicate melting and vaporization during rocky planet formation, J. Geophys. Res.: Planets **125**, e2019JE006227 (2020).

[78] C. McCoy, M. Marshall, D. Polsin, D. Fratanduono, P. Celliers, D. Meyerhofer, and T. Boehly, Hugoniot, sound velocity, and shock temperature of mgo to 2300 Gpa, Phys. Rev. B **100**, 014106 (2019).

[79] K. S. Holian, T-4 handbook of material properties data bases, Volume 1c, Equations of state, Tech. Rep. No. LA–10160-MS-VOL.1C (IAEA, Vienna, Austria, 1984).

[80] R. M. More, K. H. Warren, D. A. Young, and G. B. Zimmerman, A new quotidian equation of state (QEOS) for hot dense matter, Phys. Fluids **31**, 3059 (1988).

[81] J. T. Larsen and S. M. Lane, HYADES-A plasma hydrodynamics code for dense plasma studies, J. Quant. Spectrosc. Radiat. Transfer **51**, 179 (1994).